J|A|C|S
ARTICLES

Direct Observation of Bifunctional Electrocatalysis during CO Oxidation at Ru$_{\theta=0.37}$/Pt{111} Surfaces via Surface Stress Measurements

Larry L. Mickelson and Cody Friesen*

School of Materials, Arizona State University, Tempe, Arizona 85287

Received June 1, 2009; E-mail: cfriesen@asu.edu

Abstract: The surface stress response during the electrooxidation of CO at Pt{111}, Ru{0001}, and Ru$_{\theta=0.37}$/Pt{111} textured electrodes was studied in 0.1 M HClO$_4$ electrolytes. The surface stress signal resolves for the first time the adsorption of OH$^-$ at the CO-covered Ru{0001} surface *prior* to significant CO oxidation, a phenomenon that is not discernible in the voltammetry. The surface stress signal shows that significant tensile surface stress occurs upon oxidation of the adsorbed CO and occurs at nearly the same potential on Ru{0001} and Ru/Pt{111} surfaces. These observations demonstrate that the mechanism of bifunctionality is the OH$_{ads}$ provided to the Pt surface sites via Ru sites.

Introduction

It has been known since the 1960s that Ru−Pt alloys are more active electrocatalysts for methanol oxidation than pure Pt.[1] Later work has shown that this is also true for CO oxidation in hydrogen fuel cells where trace amounts of CO are present in the fuel stream,[2] as is often the case.[3] Even though a significant amount of work has been done to explain why Ru−Pt is more active than Pt, "the reasons are not exactly clear."[4] One possibility, known as the bifunctional mechanism, is that Ru supplies hydroxide to the CO-covered Pt sites, providing reduced oxygen species for CO oxidation.[5,6] The other possibility, known as the ligand effect, is that Ru lowers the Pt−CO binding energy of nearby Pt atoms.[7,8]

In situ high-resolution surface stress monitoring is a potentially powerful tool for the study of electrocatalysis due to the extreme sensitivity that this technique has to processes occurring at the electrode−electrolyte interface. It is important to recognize that the surface stress (f) of a solid is a fundamental thermodynamic excess quantity distinct from surface energy (γ). γ is the per unit area excess free energy required to create new solid surface at constant atomic density. The surface stress is the per unit area excess free energy required to create new solid surface at constant atom number (i.e., by elastic stretching).[9−11] Because the magnitude of both f and γ are intrinsic to the nature of the solid−electrolyte interface, the magnitude of these quantities is highly sensitive to changes in, e.g., adsorbate coverage and potential. For example, Heaton and Friesen[12] have recently used surface stress measurements to examine the oxygen reduction reaction at Pt{111} electrodes, and Mickelson et al.[13] used the same technique to examine the electrooxidation of CO at Pt surfaces. Surface stress measurements have also been used to probe a wide variety of other phenomena including DNA hybridization,[14] detection of antibodies in blood serum,[15] and contraction of artificial molecular muscles.[16] An understanding of surface stress has shed light in many other areas including thermal imaging with a bimetal oscillator,[17] corrosion of certain composite materials,[18] and structural transitions in thin magnetic films.[19]

In this work we have monitored surface stress changes as a function of potential (electrocapillarity) at three different surfaces: {111}-textured Pt thin films, {0001}-textured Ru thin films, and {111}-textured Pt thin films with Ru islands decorating the surface. The work was carried out at both clean and CO-covered interfaces. By way of introducing the work, we

(1) Bockris, J. O. M.; Wroblow, H. *J. Electroanal. Chem.* **1964**, *7*, 428–451.
(2) Niedrach, L. W.; Mckee, D. W.; Paynter, J.; Danzig, I. F. *Electrochem. Technol.* **1967**, *5*, 318.
(3) Oetjen, H. F.; Schmidt, V. M.; Stimming, U.; Trila, F. *J. Electrochem. Soc.* **1996**, *143*, 3838–3842.
(4) Bagotsky, V. S. *Fuel Cells: Problems and Solutions*; Wiley: Hoboken, NJ, 2009; p 58.
(5) Watanabe, M.; Motoo, S. *J. Electroanal. Chem.* **1975**, *60*, 267–273.
(6) Gasteiger, H. A.; Markovic, N.; Ross, P. N.; Cairns, E. J. *J. Phys. Chem.* **1994**, *98*, 617–625.
(7) Iwasita, T.; Nart, F. C.; Vielstich, W. *Ber. Bunsen. Phys. Chem.* **1990**, *94*, 1030–1034.
(8) Frelink, T.; Visscher, W.; vanVeen, J. A. R. *Langmuir* **1996**, *12*, 3702–3708.
(9) Cammarata, R. C. *Prog. Surf. Sci.* **1994**, *46*, 1–38.
(10) Cahn, J. W. *Acta Metall. Mater.* **1980**, *28*, 1333–1338.
(11) Cahn, J. W. In *Interfacial Segregation*; Johnson, W. C., Blakely, J. M., Eds.; American Society for Metals: Metals Park, OH, 1979; p 3.
(12) Heaton, T.; Friesen, C. *J. Phys. Chem. C* **2007**, *111*, 14433–14439.
(13) Mickelson, L.; Heaton, T.; Friesen, C. *J. Phys. Chem. C* **2008**, *112*, 1060–1063.
(14) Fritz, J.; Baller, M. K.; Lang, H. P.; Rothuizen, H.; Vettiger, P.; Meyer, E.; Guntherodt, H. J.; Gerber, C.; Gimzewski, J. K. *Science* **2000**, *288*, 316–318.
(15) Ndieyira, J. W.; Watari, M.; Barrera, A. D.; Zhou, D.; Vogtli, M.; Batchelor, M.; Cooper, M. A.; Strunz, T.; Horton, M. A.; Abell, C.; Rayment, T.; Aeppli, G.; McKendry, R. A. *Nat. Nanotechnol.* **2008**, *3*, 691–696.
(16) Juluri, B. K.; Kumar, A. S.; Liu, Y.; Ye, T.; Yang, Y. W.; Flood, A. H.; Fang, L.; Stoddart, J. F.; Weiss, P. S.; Huang, T. J. *ACS Nano* **2009**, *3*, 291–300.
(17) Kim, S. J.; Ono, T.; Esashi, M. *Rev. Sci. Instrum.* **2009**, *80*, 033703.
(18) Johnson, W. C.; Zhou, P.; Lucente, A. M.; Scully, J. R. *Metall. Mater. Trans. A* **2009**, *40A*, 757–767.
(19) Sander, D.; Tian, Z.; Kirschner, J. *J. Phys.: Condens. Matter* **2009**, *21*, 134015.
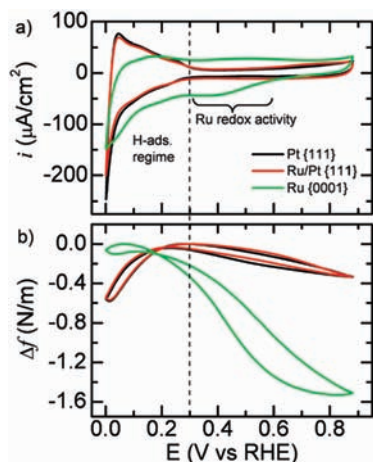
Figure 1. (a) Cyclic voltammetry and (b) electrocapillarity behavior for Pt{111} (black), Ru/Pt{111} (red), and Ru (green) in deaerated 0.1 M HClO$_4$. Scan rate 50 mV/s.

start by describing the electrocapillarity of clean surfaces and will also review the behavior of CO oxidation at Pt{111} surfaces.

Electrocapillarity. Figure 1a shows a series of voltammograms for Pt{111}, Ru{0001}, and Ru/Pt{111} electrodes in N$_2$-deaerated 0.1 M HClO$_4$ electrolyte. It is interesting to note that the Pt{111} and Ru$_{\theta=0.37}$/Pt{111} electrodes show very similar behavior, with identical hydrogen adsorption and double-layer charging characteristics. Our potential limits were chosen as 0 and 880 mV vs RHE to minimize Ru dissolution.[20] The voltammetric behavior of the Ru{0001} electrode is significantly different than those of Pt{111} or Ru/Pt{111}, with a limited degree of hydrogen adsorption and, more significantly, substantial pseudocapacitance dominated charging in the "double-layer" regime.[21] Ru is strongly oxyphilic and hence redox active in the entire potential regime, making it a prime candidate for pseudocapacitors.[22] As shown by Hadzi-Jordanov et al.[23] and Ticanelli et al.[24] OH$^-$ adsorption begins at potentials as low as 200 mV vs RHE. Comparing Ru{0001} to Ru/Pt{111} in Figure 1, it is seen that the Ru/Pt{111} electrode is significantly less oxyphilic than pure Ru.

Figure 1b displays typical electrocapillarity curves for the three electrodes studied. As was the case for the voltammetry, the Pt{111} and Ru/Pt{111} electrodes are nearly indistinguishable. However, the differences between those electrodes and Ru{0001} are substantially more pronounced than the differences observed in voltammetry. The Pt{111} and Ru/Pt{111} electrodes take on a compressive surface stress change during reversible H adsorption of −0.58 and −0.57 N/m, respectively, while the H adsorption compressive surface stress on Ru{0001} is at most −0.10 N/m, smaller by a factor of 5. In the double layer region a reversible compressive signal exists, which is −0.33 N/m on both the Pt{111} and Ru/Pt{111} surfaces, while on the Ru{0001} surface the positive-limit compressive surface

stress reaches −1.53 N/m. The significant OH$^-$ adsorption activity on Ru in this potential range results in the observation of large compressive surface stresses at positive potentials.

Experimental Section

The Pt{111} electrodes were prepared as thin films on top of a substrate consisting of a thin borosilicate glass substrate onto which a 1 nm Cr adhesion layer was deposited in ultrahigh vacuum (UHV). The Pt was deposited at 350 °C to ensure a strong {111} texture (see Supporting Information). Subsequent X-ray diffraction rocking curves showed a half-width half-maximum (HWHM) of 3.92° for the {111} peak (see Supporting Information). Atomic force microscopy (AFM) and scanning tunneling microscopy (STM) were used to investigate the sample morphology. From these images we determined the average distance between step-edges to be 2.0 nm (see Supporting Information). Ru{0001} electrodes were generated via sputter deposition of 13 nm of Ru onto a Pt{111} film. Ru/Pt{111} electrodes were synthesized by the spontaneous deposition of a submonolayer of Ru on a Pt{111} film as originally developed by Chrzanowski and Wieckowski.[25] This process is detailed later.

In situ surface stress measurements were performed using a cantilevered electrode with a capacitive sensor as described in detail elsewhere.[12] The surface stress resolution of the device is 0.016 N/m. To remove errors due to uncertainties in elastic modulus and substrate thickness (a squared term), a gravity-based calibration method was used.[12] For electrocapillarity measurements the changes in surface stress are referenced to the maximum surface stress; for CO oxidation experiments surface stress changes are referenced to the beginning of the experiment.

The Teflon cell and glassware were cleaned by soaking in hot (50 °C) nitric acid, followed by hot sulfuric acid, and finally rinsed with 18 MΩ·cm water (Barnstead Nanopure). All experiments were performed in 0.1 M HClO$_4$ (99.999%). A mercury−mercury sulfate electrode (MSE) in saturated K$_2$SO$_4$ was used as a reference (+640 mV vs SHE) for all experiments. All reported potentials have been converted to the reversible hydrogen electrode (RHE). A bridge of 0.1 M HClO$_4$ was used to prevent contamination of the electrolyte with sulfate anions. The electrolyte was deaerated with 99.999% pure dry N$_2$ gas for 8 h in a separate deaeration flask before being directly transferred into the electrochemical cell via plumbing connecting the flask and cell.

Spontaneous Deposition of Ruthenium. The protocol outlined by Wieckowski and co-workers[26,27] was used for spontaneous deposition of Ru. A solution of 0.1 M HClO$_4$ + 1 mM RuCl$_3$·3 H$_2$O (99% Alfa Aesar) was made and allowed to age for two weeks. The Pt{111} sample was placed in the solution for 3 min to allow the spontaneous deposition to occur at open circuit (∼1000 mV vs RHE). After which, the sample was rinsed with 18 MΩ·cm water and dried in a stream of N$_2$ gas. The sample was immediately reintroduced to the electrochemical cell, and the adsorbed Ru was electrochemically reduced by scanning the potential from open circuit down to 0 mV.

Extensive characterization of electrodes prepared by this process of spontaneous deposition of Ru on Pt (111) has already been done using auger electron spectroscopy (AES),[28,29] X-ray photoelectron spectroscopy (XPS),[20] and STM.[26,27,30−32] It has been shown that

(20) Kim, H.; de Moraes, I. R.; Tremiliosi, G.; Haasch, R.; Wieckowski, A. *Surf. Sci.* **2001**, *474*, L203–L212.

(21) Gasteiger, H. A.; Markovic, N.; Ross, P. N.; Cairns, E. J. *J. Phys. Chem.* **1993**, *97*, 12020–12029.

(22) Zheng, J. P.; Cygan, P. J.; Jow, T. R. *J. Electrochem. Soc.* **1995**, *142*, 2699–2703.

(23) Hadzi-Jordanov, S.; Angerstein-Kozlowska, H. V., M.; Conway, B. E. *J. Phys. Chem.* **1977**, *81*, 2271–2279.

(24) Ticanelli, E.; Beery, J. G.; Paffett, M. T.; Gottesfeld, S. *J. Electroanal. Chem.* **1989**, *258*, 61–77.

(25) Chrzanowski, W.; Wieckowski, A. *Langmuir* **1997**, *13*, 5974–5978.

(26) Crown, A.; Johnston, C.; Wieckowski, A. *Surf. Sci.* **2002**, *506*, L268–L274.

(27) Strbac, S.; Johnston, C. M.; Lu, G. Q.; Crown, A.; Wieckowski, A. *Surf. Sci.* **2004**, *573*, 80–99.

(28) Chrzanowski, W.; Kim, H.; Wieckowski, A. *Catal. Lett.* **1998**, *50*, 69–75.

(29) Tremiliosi, G.; Kim, H.; Chrzanowski, W.; Wieckowski, A.; Grzybowska, B.; Kulesza, P. *J. Electroanal. Chem.* **1999**, *467*, 143–156.

(30) Herrero, E.; Feliu, J. M.; Wieckowski, A. *Langmuir* **1999**, *15*, 4944–4948.

(31) Cram, S.; Friedrich, K. A.; Geyzers, K. P.; Stimming, U.; Vogel, R. *J. Anal. Chem.* **1997**, *358*, 189–192.
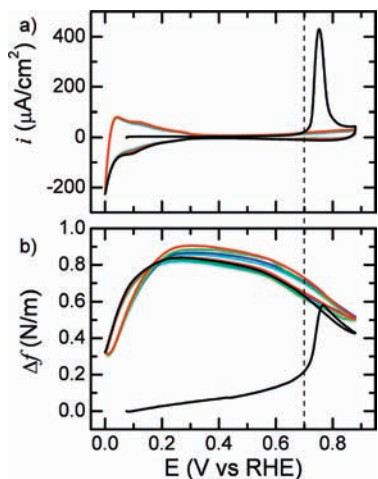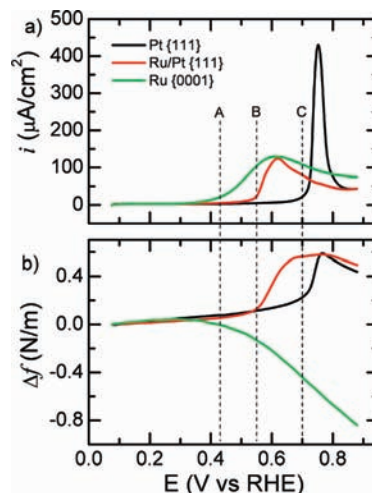
Figure 2. (a) Cyclic voltammetry and (b) electrocapillarity during (cycle 1) CO oxidation on Pt{111} (black) in deaerated 0.1 M HClO$_4$. Cycles 2−5 are red, green, blue, and cyan, respectively. Scan rate 50 mV/s. Arrow in (b) indicates first positive-going sweep. Dotted line indicates the inititation of CO oxidation.

Figure 3. (a) Positive-going linear sweep voltammetry and (b) electrocapillarity during CO oxidation on Pt{111} (black), Ru/Pt{111} (red), and Ru{0001} (green). Scan rate 50 mV/s. Dotted lines mark 20 μA/cm^2 turn-on potentials: A, B, C for Ru{0001}, Ru/Pt{111}, and Pt{111}, respectively.

the process is self-limiting and that a submonolayer coverage of Ru is obtained with islands 3−5 nm in diameter of mostly (~85%) monatomic height.[26] In this work the Ru surface coverage was determined using angle-resolved XPS (AR-XPS) to be 0.37 ± 0.07.

CO Electrooxidation Experiments. Before executing the CO oxidation experiments, 10 cycles of voltammetry were run, with potential limits of 0 and 880 mV vs RHE, to ensure the cleanliness of the sample and check for characteristic behavior, as shown in Figure 1. In order to adsorb a saturation coverage of CO on the electrode, CO was bubbled directly into the cell for 15 min while the electrode was under potentiostatic control at 75 mV. After the CO adsorption process, dissolved CO is removed from the electrolyte by bubbling N$_2$ for 3 h directly into the cell. As we have shown previously,[13] this process simultaneously ensures a saturation coverage of CO on the electrode and complete removal of CO from the electrolyte. Then, while maintaining potentiostatic control, the CO is electrooxidized by scanning the potential at 50 mV/s from 75 to 880 mV, followed by several cycles of voltammetry. As Figure 2a shows, all of the CO was oxidized during this first sweep. Earlier work[13] has shown that the Pt{111} shows a tensile surface stress during the oxidation of CO. However, as described below, the surface stress response during CO oxidation on Ru{0001} is significantly different than that of either Pt{111} or Ru/Pt{111}. The change in surface stress is not only 40% larger on Ru{0001} than on Pt{111} or Ru/Pt{111}, but is of *opposite* sign. As discussed later, these differences are explained by accounting for the oxyphilic nature of Ru. As a natural consequence of resolving these differences in surface stress during CO oxidation, the mechanism and rate-limiting step for CO oxidation become clear, including the mechanism of Ru/Pt{111} surface alloys as bifunctional electrocatalysts.

Results

Figure 3a shows the first anodic voltammetric sweep applied to the CO-covered surfaces of Pt{111}, Ru/Pt{111}, and Ru{0001}. The three CO electrooxidation voltammetric curves are qualitatively similar, but quantitatively quite different. First, the 20 μA/cm^2 turn-on potential for CO oxidation is 270 mV lower on Ru{0001} and 150 mV lower on Ru/Pt{111} than on Pt{111}, where it has a value of 700 mV vs RHE, as marked in Figure 3a with A, B, and C respectively. Second, the Tafel

(32) Friedrich, K. A.; Geyzers, K. P.; Marmann, A.; Stimming, U.; Vogel, R. *Z. Phys. Chem.* **1999**, *208*, 137–150.

slopes at the onset of CO oxidation are significantly different for Pt{111}, Ru/Pt{111}, and Ru{0001} having values of 71, 46, and 146 mV/decade, respectively; showing well-known electrocatalytic behavior, CO oxidation kinetics are much more facile on Ru/Pt{111} than on Pt{111} or Ru{0001}. Third, the current density at the positive limit, after CO oxidation, is 75% larger on Ru{0001} than on Pt{111} or Ru/Pt{111}. Fourth, the integrated charges vary, even when averaged over multiple samples, increasing from Pt{111} to Ru/Pt{111} to Ru{0001} with values of 487, 597, and 846 μC/cm^2, respectively. We will show that this large variation in CO oxidation charge is associated with background processes due to the differences in oxyphilicity of the electrodes.

Figure 3b shows the surface stress signals associated with the CO oxidation of Figure 3a. In previous work[13] it was shown that CO oxidation on Pt{111} electrodes results in a tensile surface stress; the present work on strongly {111}-textured films gives a maximum surface stress change of 0.59 N/m. A tensile surface stress of 0.58 N/m was observed during CO oxidation on the Ru/Pt{111} electrode, with the CO oxidation occurring at a lower potential. The similarity of these two surface stress signals is striking. CO oxidation on Ru{0001} gives a surface stress response of −0.84 N/m. The fact that the signal is not only larger in magnitude but also of opposite sign points to a fundamental difference between CO oxidation on Ru{0001} versus that on Pt{111} and Ru/Pt{111} surfaces, which is not discernible from the voltammetry.

The voltammetric and electrocapillarity behaviors of the electrodes are displayed in Figure 4, both before exposure to CO (black) and after a full CO-adlayer has been oxidized (red). The before-and-after electrocapillarity signals are identical within experimental reproducibility.

Deconvoluting Faradaic and Non-Faradaic Processes. As shown in Figure 5, the charge observed during CO electrooxidation is highly dependent on the electrode metal and varies by more than 70% from 487 μC/cm^2 on Pt{111} to 597 μC/cm^2 on Ru/Pt{111} to 846 μC/cm^2 on Ru{0001}. This variation is largely associated with differences in the double-layer and
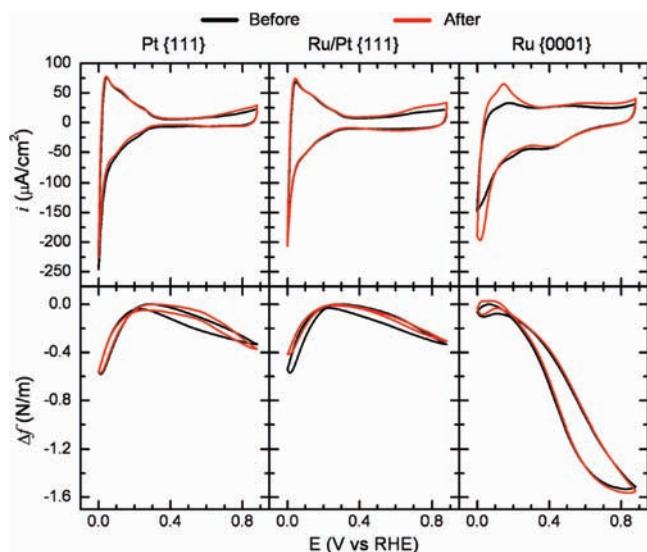
Figure 4. Voltammetry (top row) and electrocapillarity (bottom row) for Pt{111} (left column), Ru/Pt{111} (middle column) and Ru{0001} (right column) in deaerated 0.1 M HClO$_4$ both before exposure to CO (black) and after complete oxidation of a CO monolayer (red). Scan rate 50 mV/s.
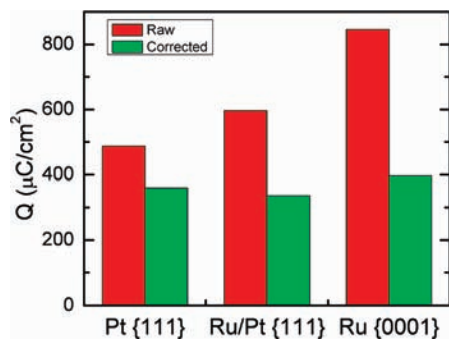
Figure 5. Faradaic charge density due to CO oxidation, raw uncorrected (red) and corrected (green), all results averaged over several samples. See text for explanation of correction model.

pseudocapacitive character of the three electrodes.[33−36] Thus, an accurate background subtraction technique is needed to extract the Faradaic charge from the measured charge for each of the electrodes.

One technique for the removal of background charge was developed by Gomez et al.[33] Their method correctly accounts for all of the pertinent contributions, resolving the apparent discrepancy between CO oxidation charges on Pt (111) single crystals in perchloric versus sulfuric acids, and allows for the accurate determination of CO saturation coverages. However, the method only concerns the initial and final states of the electrode, not the evolution of charge during the CO oxidation process. Since our interest lies in the evolution of charge and surface stress during CO oxidation, a new method of accounting for background processes was developed.

Our minimally arbitrary numerical method accounts for background charge accumulation and provides potentiodynamic

information during a Faradaic process. The only assumption in the technique is that the background current is a coverage-based average of background currents characteristic of the initial and final interfaces. For this specific work, the charge accumulation is initially set by the CO-covered interface, i_1, and evolves in a coverage-dependent way to that characteristic of the final CO-free interface, i_2, as determined iteratively by the integrated Faradaic charge:

$$i_b = i_1 + (i_2 - i_1)\frac{Q_i}{Q_{Tot}} \tag{1}$$

where i_b is the calculated background current density across the potential range of interest during a voltammetric scan; Q_i is the charge of the Faradaic process at a given potential; and Q_{Tot} is the total charge of the Faradaic process. We note the mathematical similarity of this method to background subtraction in the field of surface science[37] but point out that the physical meanings of the subtraction in the two fields are unconnected. By noting that $Q_i/Q_{Tot} = 1 - \theta_{CO}/\theta_{CO,sat}$ and defining $\theta' = \theta_{CO}/\theta_{CO,sat}$ we can rewrite eq 1 as

$$i_b = i_1\theta' + i_2(1 - \theta') \tag{2}$$

showing that the net background current density, i_b, is simply a weighted average of i_1 and i_2 where the weighting function, θ', is the fraction of the interface covered by CO.

The iterative implementation of our background subtraction technique initiates with i_b equal everywhere to i_1, allowing calculation of Q_i and Q_{Tot}. These charges are then used to calculate a new background using eq 1, and the process is iterated to convergence. The robustness of this iterative process is indicated by its rapid convergence. In all cases a self-consistency of better than 0.1% was reached after five iterations, as seen in the Supporting Information. Code to perform this deconvolution numerically can be found online.[38]

Figure 5 shows the integrated CO oxidation charge after background subtraction for the three electrodes. The variation in corrected CO oxidation charge by sample type is small, the values of which are 360, 337, and 397 μC/cm^2 for Pt{111}, Ru/Pt{111}, and Ru{0001}, respectively. Thus, the saturation coverage of CO on our Pt{111} sample is 0.74 ML (360 μC/cm^2/486 μC/cm^2·ML). Gomez et al.[33] report a saturation coverage 0.67 ML for CO on Pt(111) single crystals in 0.1 M HClO$_4$. The nonzero step-edge density of our polycrystalline samples makes it necessary to include step-edge adsorption effects when comparing coverages. Luo et al.[39] used temperature programmed desorption (TPD) experiments on Pt(S)[4(111) × (100)] (i.e., Pt(335)) to determine the coverage of CO at step and terrace sites. At saturation the contribution of CO$_{ads}$ at step sites was 0.25, but since one-in-four of the adsorption sites were steps, the occupation of step sites was 1.0. On the bases of these results from single crystal work, an average step-edge distance of 2.0 nm for our samples, and a step-edge width of 0.28 nm (the Pt−Pt distance), we calculate an expected CO saturation coverage of 0.72, which we consider in reasonable agreement with our measured value of 0.74.

(33) Gomez, R.; Feliu, J. M.; Aldaz, A.; Weaver, M. J. *Surf. Sci.* **1998**, *410*, 48−61.
(34) Climent, V.; Garcia-Araez, N.; Herrero, E.; Feliu, J.; Russ, J. *Electrochemistry* **2006**, *42*, 1145−1160.
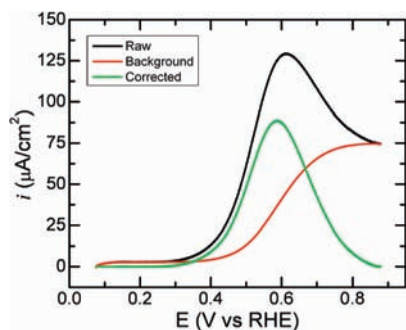(35) Cuesta, A. *Surf. Sci.* **2004**, *572*, 11−22.
(36) Orts, J. M.; Fernandezvega, A.; Feliu, J. M.; Aldaz, A.; Clavilier, J. *J. Electroanal. Chem.* **1992**, *327*, 261−278.

(37) Shirley, D. A. *Phys. Rev. B* **1972**, *5*, 4709−4714.
(38) Friesen Research Group: http://friesen.asu.edu/code.html (accessed May 5, 2009).
(39) Luo, J. S.; Tobin, R. G.; Lambert, D. K.; Fisher, G. B.; Dimaggio, C. L. *Surf. Sci.* **1992**, *274*, 53−62.

Figure 6. CO oxidation by positive-going linear sweep voltammetry on Ru{0001} in deaerated 0.1 M HClO₄. Legend: original, raw current (black); background current (red); corrected, Faradaic current (green). Scan rate 50 mV/s.

Figure 6 shows the efficacy of this method for deconvoluting the Faradaic and background contributions. The raw current, shown in black has an asymmetric shape, making it difficult to determine the peak width with a full-width at half-maximum (fwhm) criteria. However, after subtracting the background current (shown in red), the remaining current (shown in green) has a symmetric Gaussian shape, making it clear that the peak width is 205 mV on Ru{0001} (fwhm for Ru/Pt{111} and Pt{111} are 129 and 37 mV, respectively, Figures S2 and S3, Supporting Information). It is noted again that this technique represents a *minimally arbitrary* method for background subtraction, where the only input is the selection of a potential window for analysis.

Using the same Faradaic/background deconvolution technique it is also possible to remove the background contributions to the surface stress signal. By applying the same coverage-linear relationship assumption for surface stress as was earlier applied to current density, we are able to extract the portion of the surface stress signal that is due only to CO oxidation. This method for deconvoluting the CO oxidation surface stress ($f_i^{\text{CO-oxid}}$) from the electrocapillarity surface stress is given as

$$f_i^{\text{CO-oxid}} = f_i^{\text{raw}} - f_i^{\text{ECAP}} \cdot Q_i / Q_{\text{Tot}} \qquad (3)$$

where f_i^{raw} is the raw surface stress signal during CO oxidation, f_i^{ECAP} is the electrocapillarity behavior of the sample before exposure to CO (Figure 1b), and Q_i and Q_{Tot} have the same meanings as expressed in eq 1 and shown graphically in Figure 7a.

Figure 7b displays f_i^{raw}, f_i^{ECAP}, and $f_i^{\text{CO-oxid}}$ for the Ru{0001} electrode (other electrodes shown in Supporting Information). It is seen that the corrected surface stress signal (green curve), is due entirely to the CO oxidation process and that it follows the raw signal (black curve) until oxidation of CO begins, at which point it diverges from the raw signal in the tensile direction. This correction clearly shows that even though the *apparent* surface stress change due to CO oxidation on Ru{0001} surfaces is compressive the *actual* surface stress change associated with CO oxidation is tensile.

Figure 8a shows corrected surface stress data ($f_i^{\text{CO-oxid}}$) for the Pt{111}, Ru/Pt{111}, and Ru{0001} surfaces. As can be seen in Figure 3, the raw surface stress signal during CO oxidation is tensile on Pt{111} and Ru/Pt{111}, but compressive on Ru{0001}. However, after accounting for double-layer effects (Figure 8a) the surface stress due to CO oxidation is tensile on Pt{111}, Ru/Pt{111}, and Ru{0001} (0.80, 0.84, and 0.63 N/m respectively). At potentials below 550 mV, the Pt{111} and
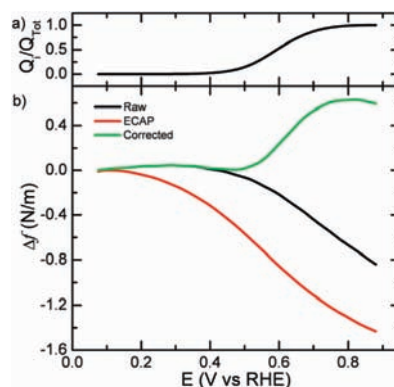
Figure 7. (a) Corrected Faradaic CO oxidation charge. (b) Surface-stress during CO oxidation in deaerated 0.1 M HClO₄: raw CO oxidation surface stress (black), CO-free electrocapillarity (red), corrected CO oxidation surface stress (green). Working electrode Ru{0001}. Scan rate 50 mV/s.
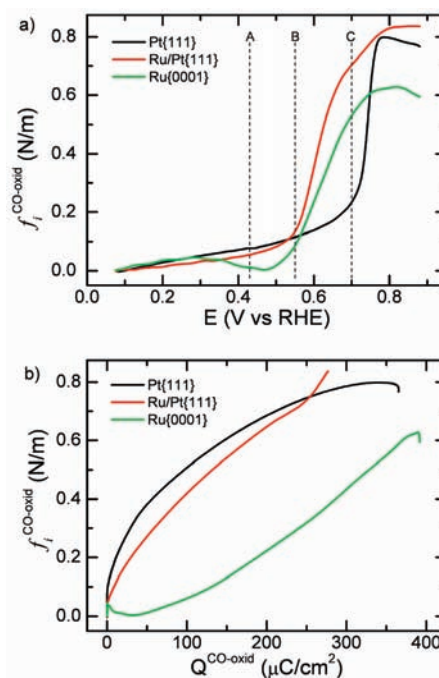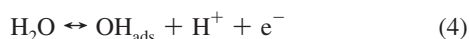

Figure 8. Corrected CO oxidation surface stress in deaerated 0.1 M HClO₄ as ordinate on Pt{111} (black), Ru/Pt{111} (red), and Ru{0001} (green). Scan rate 50 mV/s. (a) Potential as abscissa. (b) Corrected CO oxidation charge density as abscissa. Dotted lines in (a) mark turn-on potentials taken from Figure 3. A, B, and C refer to Ru{0001}, Ru/Pt{111}, and Pt{111}, respectively.

Ru/Pt{111} corrected surface stress signals are nearly identical, both having a small positive slope. At potentials above 700 mV, CO oxidation begins on the Pt{111} electrode with the observation of a large monotonic tensile surface stress trend. A similar feature is observed on the Ru/Pt{111} electrode, but at a significantly more negative potential of 550 mV, a *direct* observation of bifunctional electrocatalysis. Interestingly, the corrected Ru{0001} signal follows the Pt{111} and Ru/Pt{111} signals until 300 mV, at which point a small compressive surface stress sets in. At 470 mV it reaches a minimum, and using the surface stress−potential slope at the CO oxidation turn-on potential on Pt{111} and Ru/Pt{111} (2.3 and 2.2 N/m·V, respectively), the Ru{0001} turn-on potential for significant CO oxidation is 552 mV. Figure 8b is a parametric plot of CO oxidation surface stress against Faradaic CO oxidation charge. Against a charge axis, the Pt{111} and Ru/Pt{111} surfaces

behave similarly; with an immediate tensile trend associated with the removal of CO, the surface stress change per CO molecule is similar on Pt{111} (1.52 eV/CO, evaluated at 10 μC/cm^2; 0.62 eV/CO at 50 μC/cm^2) and on Ru/Pt{111} (1.15 eV/CO at 10 μC/cm^2; 0.66 eV/CO at 50 μC/cm^2). As was also seen in Figure 8a the Ru{0001} surface initially trends compressive, and turns tensile only after 8% of the CO oxidation charge is passed (with a surface stress change per CO molecule of 0.10 eV/CO, evaluated at 50 μC/cm^2).

Discussion

The major result of this work is contained in Figure 8, with the direct observation of bifunctional electrocatalysis and, as will be described below, the elucidation of the bifunctional mechanism. Gasteiger et al.[6] have proposed a mechanism for the oxidation of adsorbed CO, which proceeds in two steps,

$$H_2O \leftrightarrow OH_{ads} + H^+ + e^- \qquad (4)$$

followed by

$$CO_{ads} + OH_{ads} \leftrightarrow CO_2 + H^+ + e^- \qquad (5)$$
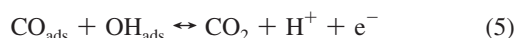
where CO_{ads} and OH_{ads} denote adsorbed species. The surface stress data from Figure 8 and reactions 4 and 5 provide a framework for the progression of CO oxidation. From the compressive surface stress on the Ru{0001} surface in the potential range 285−470 mV it is clear that at these potentials the charge is dominated by the OH$^-$ adsorption described by reaction 4. Thus, the compressive feature in the surface stress between 285 and 470 mV is due to OH$^-$ adsorption occurring *before* CO oxidation occurs to any significant extent, a detail that is not observable with voltammetry, but is clearly elucidated via the highly interfacial sensitive surface stress measurements. This OH$^-$ adsorption before CO oxidation behavior is likely the origin of the observed large activation regime on CO-covered Ru{0001} surfaces (~200 mV) and the large Tafel slope in this regime. It is also clear that the Ru submonolayer of the Ru/Pt{111} surface has lost some of it is oxyphilic character with the initial compressive surface stress associated with OH$^-$ adsorption being absent on Ru/Pt{111} electrodes.

Significant CO oxidation, reaction 5, is easily defined by voltammetry on Pt{111} and Ru/Pt{111} with turn-on potentials of 700 and 550 mV, respectively. Picking a turn-on potential for reaction 5 on Ru{0001} is more involved. From the raw voltammetry a turn-on potential of 427 mV is determined. However, as the compressive trend in the corrected surface stress shows (Figure 8a), reaction 5 is not proceeding to any significant extent at this potential. Hence, it would be instructive to use the corrected surface stress as a guide in the selection of a turn-on potential. On Pt{111} and Ru/Pt{111} the slope of corrected surface stress vs potential at their turn-on potentials is nearly the same, with values of 2.3 and 2.2 N/m·V respectively. Taking this value as a criteria for the turn-on potential of reaction 5 on Ru{0001} gives 552 mV, only 2 mV from the turn-on potential

of Ru/Pt{111}. Unlike Ru{0001} where CO oxidation only begins after significant OH$^-$ adsorption, on the Ru/Pt{111} electrode CO oxidation proceeds immediately upon OH$^-$ adsorption, resulting in a monotonic tensile surface stress trend. Voltammetry shows that CO oxidation occurs at lower potentials and with less activation (i.e., lower Tafel slope) on Ru/Pt{111} than Ru{0001} and Pt{111}. But only surface stress shows that CO oxidation begins on the Ru/Pt{111} and Ru{0001} electrodes at effectively the same potential (the apparent difference with voltammetry is 120 mV). Hydroxide adsorption on Pt{111} surfaces begins at much higher potentials of 700 mV, and as for the case of Ru/Pt{111}, CO oxidation immediately follows OH$^-$ adsorption.

As evidenced by the lack of significant CO oxidation on Ru{0001} during early stages of OH$^-$ adsorption, reaction 5 is the rate-limiting step on Ru{0001}. On Ru/Pt{111} and Pt{111} there is no potential difference between when OH$^-$ adsorption and CO oxidation are observed, showing that on these surfaces reaction 4 is likely the rate-limiting reaction. Independently, reaction 4 occurs at low potentials on Ru{0001}, and reaction 5 is fast on Pt{111}. But, OH$^-$ adsorption only occurs at high potentials at Pt{111} surfaces. Thus, as measured by voltammetry (turn-on potentials and Tafel slopes) and surface stress (the potential at which a tensile surface stress characteristic of CO oxidation starts), bifunctionality at the Ru/Pt{111} surface is provided by the oxyphilicity of the Ru atoms supplying OH$_{ads}$ to the CO-covered Pt atoms.

Summary

Voltammetry and electrocapillarity measurements were performed on Pt{111}, Ru/Pt{111}, and Ru{0001} electrodes in 0.1 M HClO$_4$ electrolyte. A method for deconvoluting both the current and surface stress of simultaneous Faradaic and non-Faradaic processes was developed. The application of this deconvolution method to CO oxidation experiments directly elucidates the bifunctional mechanism of CO oxidation on Ru/Pt{111} surfaces. Additionally, the rate-determining step was shown to be OH$^-$ adsorption on Pt{111} and Ru/Pt{111}, whereas it is CO oxidation on Ru{0001}.

Supporting Information Available: XRD results measuring texture of Pt{111}. AFM and STM images of surface morphology. Details of AR-XPS analysis. Figure showing stability and convergence of numerical method. Corrected voltammetry for Pt{111} and Ru/Pt{111}. Surface stress correction process shown graphically. This material is available free of charge via the Internet at http://pubs.acs.org.

JA904432C